

Automatic Structural Brain Registration Using Finite Elements and Active Surfaces

Carl Lederman¹, Anand Joshi², Ivo Dinov², John Darrell Van Horn², Allan Garcia¹, Kevin Chan¹, Luminita Vese¹,
and Arthur Toga²

¹Department of Mathematics, University of California Los Angeles, CA 90095, USA

²Laboratory of Neuro Imaging, UCLA School of Medicine, Los Angeles, CA 90095, USA

Abstract:

We introduce a new volumetric registration method that effectively combines active surfaces with the finite element method. The method is able to incorporate automatic structural segmentation results to produce an anatomically accurate registration. This is not done by morphing individual regions independently, but by morphing all anatomical regions simultaneously. We explain how this approach yields better registration results than what can be obtained by either morphing the brain without region labels or by morphing each anatomical region independently. The method also effectively limits changes in volume, stretch, and shear to only what is necessary to match two images. The registration is obtained by finding the minimum of a single energy functional.

Introduction:

Image registration can refer to any means of comparing the data in different images. For example, image registration can include methods for taking several low quality images of the exact same scene and combining them to create a single high quality image [18]. But here we focus exclusively on the type of registration method that takes an initial, or template, image and morphs into to a target, or reference, image. The deformation that occurs during the morphing is taken as a direct measure of how the images are different ([3], [29] and [33]). The two images that are compared are usually two instances of the same type, such as brain MRI from two different people.

One popular class of image registration methods involves fluid dynamics ([3]). In these methods, a velocity vector field is computed based on the differences between two images and then a Navier-Stokes equation is solved in order to find a displacement field that corresponds to that vector field. In the original formulation ([3]), this results in a large variance in the local deformations that is not justified by the image differences. In [33], the formulation was modified using mutual information to prevent an unjustified variability in local volume changes.

Another class of registration methods stem from segmentation methods that have been adapted to work for registration ([15], [31]). In [15], an adaptation from the segmentation model [2], the boundary of the initial region is associated with the zero iso-contour of a level set and the level set is evolved so that it is positive on top of the target region and negative outside of the target region. The regularization term no longer acts upon the location of the level set itself, as is the case in segmentation, but on the map from the initial state to the target state. It was shown to give comparable results to the fluid based methods in its ability to register disparately shaped regions [15]. We use a variant of this active contour, or active surface in 3D, registration in the method proposed here.

The direct relationship between image segmentation and registration has led some registration methods to be promoted as joint segmentation and registration methods ([15], [31], [22] and [35]). However, any registration method, whether adapted from a segmentation method or not, can be used for segmentation, simply by ignoring the map and taking the final location of the morphing. The converse is not true. Not all segmentation methods can be easily adapted to registration, such as those involving non-differentiable level sets [17] and machine learning [30]. And even if a segmentation method can be adapted for registration, it may give a weaker segmentation result. For example, [2] can change topology and the adapted registration method [15] cannot. So while combining segmentation and registration may offer some advantages, applying a sophisticated segmentation program in advance of the registration has the potential to give a better final result. In brain registration, some segmentation preprocessing is usually applied to improve the registration result, such as stripping away the skull and non-brain tissue ([12] and [20].) The method proposed here takes advantage of much more advanced preprocessing to improve the registration result.

Many of the registration methods derived from fluid and segmentation models employ finite differences and not finite elements. Finite difference methods seem to be a natural choice as they can be immediately run on the rectangular images while finite element methods are typically used for solving PDEs on domains with complicated

boundaries. Yet for many registration applications, there are one or more objects with sharply defined boundaries within image that is to be registered. The sharp contrasts at the boundary of the object within the image are the primary driver of the registration and not the subtle variations in pixel or voxel intensities within the object. The objects are placed in a box for reasons related to the capture and storage of the image. As long as the object of interest is fully inside the image, the boundary of the image has no real significance and there is no necessity to satisfy some type of boundary condition on the image boundary. In contrast, the boundary of the object to be registered is of fundamental importance to the registration as that is what is being evolved during the morphing. But the object to be morphed is never rectangular. Finite elements have been used in engineering and computer graphics for decades [8], [9] and are a better choice for solving PDEs on an arbitrary domain.

Another relevant advantage of finite elements is that they are excellent at modeling deformation ([9] and [28]). The deformation on an element can be computed directly from the relative positions of the nodes of an element. In contrast, for finite differences, deformation is computed by approximating derivatives of a displacement field defined on a grid.

Some papers have employed volumetric finite elements, such as [6], [12], [20], [1], [7], and [24]. All of these methods are, at their core, a two step procedure in which the desired behavior of the boundary is found first and independently and then applied as a boundary term for a volumetric finite element model. The result is that the boundary nodes end up close to where the boundary matching determines they should be and a reasonable volumetric morph is produced, that is, one that does not have excessively large deformations or inverted elements. The method proposed here is distinct in its capacity to effectively combine a surface matching term and a volumetric regularization term in a single formulation to dramatically improve both the surface registration and volume registration.

We explain in the methods section how the proposed method is able to match boundaries that may initially be nowhere near each other, minimize volumetric deformation, and efficiently incorporate an arbitrary number of labels into a single coupled registration. We believe these advantages are important for the theoretical study of image registration and also may have practical benefits for the study of neurological disease. The method allows information from automatic structural segmentations to be efficiently incorporated into a single registration. The region to region interaction produce a better registration result than can be achieved by registering the regions independently and combining the registrations together in a second step. Second, the ability of the registration method to avoid deformation that is not necessary to match images may have applications to morphometry and the study of Alzheimer's disease. Any analysis of the deformation should point to meaningful differences between the brains and not merely artifacts of the registration method.

An additional practical and theoretical advantage of the method presented here is that it is a pure optimization method. The registration result is given by attempting to find the minimum of a single energy functional. Some, although not all, registration methods have this property. Optimization problems are well studied and many efficient means of finding an energy minimum have been developed, such as the Sobolev Gradient Method ([14] and [23]).

The details of the registration method are given below and three examples are given. The first two examples are used to explain two very important aspects of the registration method and should not be misinterpreted as the maximum to which method is capable. The third example registers brains that have been automatically segmented using a modern machine learning based method. We explain how it achieves the desired registration that matches all labels and minimized deformation. In future studies, we will evaluate the registration method using manual markers which are hidden to the registration method and do a morphometric analysis of healthy and Alzheimer's disease patients. Both of these future studies will depend not just on the quality of the registration method but also on the segmentation quality and statistical methods used to analyze the morphometry.

Methods:

Starting from a raw image or volume, existing software must be applied that can segment the images into regions of interest. For the case of the 3D brain MRI, we remove the skull and non-brain tissue, and use a computer learning based method [30] to automatically identify 56 anatomical regions in each brain. The method proposed here will use these region labels to guide the registration.

A single tetrahedral mesh with multiple smooth region labels must then be constructed from the initial segmented image. Tetrahedral mesh generation is not a straightforward task and is a current active area of research. For most methods, mesh generation is generally a two step process. First, construct a web of region boundaries from the images. Second, fill in the region boundaries with tetrahedra. The first step can fail for automatically segmented data. Some unusual feature of the image can cause two boundaries to intersect and consequently the mesh generation to fail. Thus the method described in [16], (available online at <http://www.nitrc.org/projects/tmma>) is used which can generate a mesh directly from the images. It also has a number of other desirable properties, such as adaptively sized tetrahedra with boundary tetrahedra of sub-voxel resolution, good tetrahedra dihedral angles, smooth regions boundaries (i.e., not voxelized), and a multi-resolution representation. All of these properties are essential to making the registration method presented here work adequately.

During registration, the mesh is deformed from an initial state X , to a morphed state x . The change in the mesh from the initial to the morphed state is described by a displacement vector field v :

$$(1) \quad v = x - X$$

The registration result is achieved by obtaining an optimal displacement vector field v that minimizes a specific energy functional $G(v)$. The energy functional consists of the sum of two terms, an elastic regularization term $E(v)$ and a novel data fidelity term, $A(v)$, that is minimized when the morphed regions and target regions have the same shapes and occupy the same positions. To find the minimum energy, an artificial time is introduced and the whole mesh deforms to decrease the energy at each time step.

The fidelity term $A(v)$ is formulated using level sets as is also done in [15]. The boundary of every region coincides exactly with the zero iso-contour of a corresponding level set. The level sets are linear on each element. Unlike what is commonly practiced, the level sets in our formulation are only utilized on their respective regions and not on the whole domain. Without this, the amount of computation required would increase dramatically as the number of regions increases. This does inhibit a topological change which is important for many level set applications, but this is not an issue here as topological change may not be appropriate if the initial and target volumes have homologous features, as the automatically segmented brain volumes do.

Multiple level sets exist for multiple regions and the level sets are sewn together at the boundaries. This prevents regions from overlapping and gaps from developing. This also allows regions to interact during the morphing. If one region moves to a given location, it will necessarily pull all neighboring regions along with it. Given N anatomical brain regions and their boundaries, we define the functions

$$(2) \quad \varphi_0(x) = \text{distance to nearest boundary}$$

$$\varphi_{0,m}(x) = \begin{cases} \varphi_0(x) & \text{if } x \text{ is in region } m \\ 0 & \text{otherwise} \end{cases}$$

The initial level sets that are exactly zero on the boundary of the smooth regions are provided as a byproduct of the meshing method [16].

The target regions are obtained directly from the segmented target image without any smoothing. This is computationally faster than using a smoothed out version of the target of image, though this may be something we reconsider in a future work. We define

$$(3) \quad I_m(x) = \begin{cases} m & \text{if } x \text{ is in region } m \\ 0 & \text{otherwise} \end{cases}$$

From these functions an energy is constructed that will work if an initial and target region have little or no overlap. This is not problematic when only one region is being registered as a rigid alignment can be performed ahead of time. But with a large number of regions, there is no guarantee that all regions in the initial and target images will overlap. If an initial and target region do not overlap, a penalty is added for the initial region being

small. This has the effect of causing the initial region to grow in volume during the morphing until it overlaps significantly with the target region and then collapse on it. The following quantity M_m is a measure of how well the region being morphed covers the corresponding target region:

$$(4) M_m = \frac{\int H(\varphi_{0,m}(x - v(x)))I_m}{\int I_m} \in [0,1]$$

Based on the above remarks, we define the functional $A(v)$ as:

$$(5) A(v) = \sum_{m=1}^N \int \delta(I_m - m)(1 - H(\varphi_{0,m}(x - v(x)))) + M_m \int (1 - \delta(I_m - m))H(\varphi_{0,m}(x - v(x))) \\ + (1 - M_m) \int (1 - \delta(I_m - m))(1 - H(\varphi_{0,m}(x - v(x))))$$

Typically, other segmentation and registration methods of this type ([2], and [15]) are implemented with smooth approximations to the Heaviside and Delta functions. This will cause the fidelity term to affect the deformation in region interiors. However, with finite elements, accurate modeling of two dimensional surfaces imbedded in three dimensional space is possible. The proposed method takes advantage of this by having the fidelity term only affect region boundaries while leaving region interiors free to position themselves in a deformation minimizing configuration.

On the other hand, a somewhat smooth Heaviside function does have some advantages. It prevents the mesh from acquiring sharp features from the voxelization in the target image (the voxelization is a byproduct of how the image is captured and stored) and improves numerical stability. The mesh connectivity is employed to create some smoothing along the exact two dimensional boundary. Since the smoothing is not volumetric, all the advantages described in the previous paragraph are maintained.

Additionally, this region matching formulation allows mesh region boundaries freedom to move along boundaries in the target region without penalty. This type of boundary movement may be necessary to match other areas of the image or reduce deformation.

We also note that the term $A(v)$ requires the same labels to occur in both the target and initial image for a sensible registration. This usually is the case for medical imaging applications as all human beings generally have the same anatomy. But there are certainly interesting problems where this is not the case, such as when a healthy brain is compared to a brain with a tumor. Cases like this may be of interest but are outside the scope of this registration method (as well as most others).

The second part of the energy functional, $E(v)$, is designed to resist deformation. The deformation of the tetrahedral mesh is computed using the deformation gradient F :

$$(6) F = \frac{dx}{dX}$$

The displacement vector field v is related to F by:

$$(7) \nabla_x v = I - F^{-1}$$

However, it is far better to compute F directly from the node locations of an element ([28],[9]). If the four nodes of a tetrahedron are given the superscripts a,b,c,d and subscripts $1,2,3$, for the coordinates of a node in three dimensional space:

$$(8) \quad dx = \begin{bmatrix} x_1^b - x_1^a & x_1^c - x_1^a & x_1^d - x_1^a \\ x_2^b - x_2^a & x_2^c - x_2^a & x_2^d - x_2^a \\ x_3^b - x_3^a & x_3^c - x_3^a & x_3^d - x_3^a \end{bmatrix},$$

$$dX = \begin{bmatrix} X_1^b - X_1^a & X_1^c - X_1^a & X_1^d - X_1^a \\ X_2^b - X_2^a & X_2^c - X_2^a & X_2^d - X_2^a \\ X_3^b - X_3^a & X_3^c - X_3^a & X_3^d - X_3^a \end{bmatrix},$$

$$F = dx dX^{-1}$$

Another useful measure of deformation is C , the Right Cauchy-Green deformation tensor, which is unaffected by rotation and defined by:

$$(9) \quad C = F^T F$$

In three dimensional space, there are exactly three invariants of deformation. These invariants relate to volume change, shear, and stretch. If $\lambda_1, \lambda_2, \lambda_3$ are the eigenvalues of F , then a choice for the three invariants is:

$$(10) \quad J_1^C = \text{tr}(C) = \lambda_1^2 + \lambda_2^2 + \lambda_3^2,$$

$$J_2^C = \frac{1}{2} (\text{tr}(C)^2 - \text{tr}(C^2)) = \lambda_1^2 \lambda_2^2 + \lambda_1^2 \lambda_3^2 + \lambda_2^2 \lambda_3^2$$

$$J_3^C = \det(C) = \lambda_1^2 \lambda_2^2 \lambda_3^2$$

The regularization energy is the Mooney-Rivlin elasticity [21], which is a function of all three invariants:

$$(10) \quad W = k_1 J_1^C + k_2 J_2^C + g(\sqrt{J_3^C})$$

If a change in all three of these invariants is resisted, measurements taken of them should relate to meaningful differences between the initial and target images and not just be artifacts of the registration method. For example, if volume change is resisted but not stretching, unnecessary stretching may occur minimize volume change.

The Mooney-Rivlin model also provides an accurate elastic model over a wider range of deformations in comparison to simpler models such as the St. Venant Kirchoff.. This is important for the method proposed here in particular as the fidelity term may cause considerable expansion in regions before they contract. It also provides more general advantages to numerical stability and it may simply be necessary to allow large deformations as they could potentially be required to match the initial and target image if the images differ substantially in some areas. Additionally, the Mooney- Rivlin elasticity, unlike the St. Venant Kirchoff elasticity and even the Neo-Hookean elasticity is polyconvex [21]. This is a desirable property for optimization problems like the one presented here.

We chose a specific formulation such that the undeformed state is a stable equilibrium and reasonable elastic behavior is achieved for our registration method.

$$(11) \quad W = \frac{\mu}{2}(\text{tr}(C)) + \frac{\mu}{2} \left(\frac{1}{2} \text{tr}(C)^2 - \text{tr}(C^2) \right) + 3\mu(\det(F) - 1)(\det(F) - 2)$$

$$+ 4\lambda(\det(F) - 1)^2 \quad \text{if} \quad \det(F) < 1$$

$$W = \frac{\mu}{2}(\text{tr}(C)) + \frac{\mu}{2} \left(\frac{1}{2} \text{tr}(C)^2 - \text{tr}(C^2) \right) + 3\mu(\det(F) - 1)(\det(F) - 2) \quad \text{if} \quad \det(F) \geq 1$$

The total energy is given by:

$$(12) \quad G(v) = A(v) + E(v) \quad \text{where} \quad E(v) = \int W(\nabla v)$$

The L^2 gradient of the functional is:

$$(13) \quad \nabla_{L^2} G(v) = - \sum_{m=1}^N \left\{ \begin{array}{l} \delta(\varphi_{0,m}(x - v(x))) \nabla_x (\varphi_{0,m}(x - v(x))) \quad \text{if} \quad I_m(x) = m \\ (1 - 2M_m) \delta(\varphi_{0,m}(x - v(x))) \nabla_x (\varphi_{0,m}(x - v(x))) \quad \text{if} \quad I_m(x) = 0 \end{array} \right.$$

$$- \text{div} \left(\frac{dW}{dF} \right)$$

$$\frac{dW}{dF} = \mu F + \mu F(\text{tr}(C)I - C) + 3\mu(2 \det(F) - 3) \det(F) F^{-T}$$

$$+ 8\lambda(\det(F) - 1) \det(F) F^{-T} \quad \text{if} \quad \det(F) < 1$$

$$\frac{dW}{dF} = \mu F + \mu F(\text{tr}(C)I - C) + 3\mu(2 \det(F) - 3) \det(F) F^{-T} \quad \text{if} \quad \det(F) \geq 1$$

The minimum can be found by taking:

$$(14) \quad \frac{dv}{dt} = -\nabla_{L^2} G(v)$$

However, an adjustment is made to improve the numerical implementation. Solving equation (14) involves computing the gradient of the level set on the deformed mesh. This can be done directly by the formula:

$$(15) \quad \nabla_x \varphi_{0,m} = \begin{bmatrix} \frac{d\varphi_{0,m}}{dx_1} \\ \frac{d\varphi_{0,m}}{dx_2} \\ \frac{d\varphi_{0,m}}{dx_3} \end{bmatrix} \quad d\varphi_{0,m} = \begin{bmatrix} \varphi_{0,m}(x^b) - \varphi_{0,m}(x^a) \\ \varphi_{0,m}(x^c) - \varphi_{0,m}(x^a) \\ \varphi_{0,m}(x^d) - \varphi_{0,m}(x^a) \end{bmatrix}$$

$$\nabla_x \varphi_{0,m} = dx^{-T} d\varphi_{0,m}$$

As the elements flatten, the matrix dx approaches uninvertibility and the derivatives computed approach infinity. Theoretically, the elastic energy should approach infinity at a sufficient rate to prevent any inversion. But while this should work theoretically, it gives disastrous results when implemented numerically. The elastic energy in equation (11) is bounded near 0. To keep the calculated derivatives small for nearly flattened tetrahedra, the inverse matrix in equation (15) is replaced with an approximation to the Moore–Penrose pseudo-inverse (with ε a small positive constant) :

$$(16) \quad \overline{dx}^{-1} = (dx^T dx + \varepsilon I)^{-1} dx^T$$

Approximating the inverse of a matrix in this way is known as Tikhonov regularization [27], which is typically used in solving linear systems involving uninvertible matrices. The effect of Tikhonov regularization can be seen using SVD decomposition.

$$(17) \quad dx = U \Sigma V^T$$

where U and V are rotation matrices and Σ is diagonal matrix whose diagonal entries are the singular values of dx , σ_1 , σ_2 , σ_3 (the absolute value of the eigenvalues). The inverse is given as the product of U, V , and diagonal matrix D :

$$(17) \quad V D U^T$$

where

$$(19) \quad D_{ii} = \frac{1}{\sigma_i}$$

for the true inverse

$$(20) \quad \begin{aligned} D_{ii} &= \frac{1}{\sigma_i} \quad \text{if} \quad \sigma_i \neq 0 \\ D_{ii} &= 0 \quad \text{if} \quad \sigma_i = 0 \end{aligned}$$

for the Moore-Penrose pseudo-inverse and

$$(21) \quad D_{ii} = \frac{\sigma_i}{\sigma_i^2 + \varepsilon}$$

for the pseudo-inverse approximation.

In directions where the deformed tetrahedra have sufficient length, in comparison to ε , the derivative approximation is close to the true derivative. In directions where the tetrahedra are nearly flattened, a very large derivative is replaced with a very small one. Thus the elasticity component of the L^2 gradient should always be able to prevent the active contour component of the L^2 gradient from causing an element to invert.

While equation (14) with the modification in equation (16) could be used to obtain the minimum of functional (12), the Sobolev Gradient Method is faster. As discussed in [14] and [23], it can be implemented by replacing equation (14) with:

$$(22) \quad \frac{dv}{dt} = -\nabla_{H^1} G(v) = -(1 - K\Delta)^{-1} \nabla_{L^2} G(v)$$

For this particular optimization problem, better results are obtained by taking a larger value of K . Increasing the value of K causes additional smoothing, which may be beneficial because the L^2 gradient is not at all smooth. It is very large on region boundaries and small on region interiors.

The solution, i.e. the v that minimizes equation (12), is found at 3 resolutions. The registration is first completed at a low resolution where both the initial and target images have 1/64 the number of voxels. This results in fewer tetrahedra and larger time steps, allowing the solution to be found hundreds of times faster than at the highest resolution. The final location of a low resolution registration is then used as the starting position of a registration at a higher resolution. The undeformed state X is not the starting position of the registration at a given resolution, but the high quality mesh created from the initial image.

Results and Discussion:

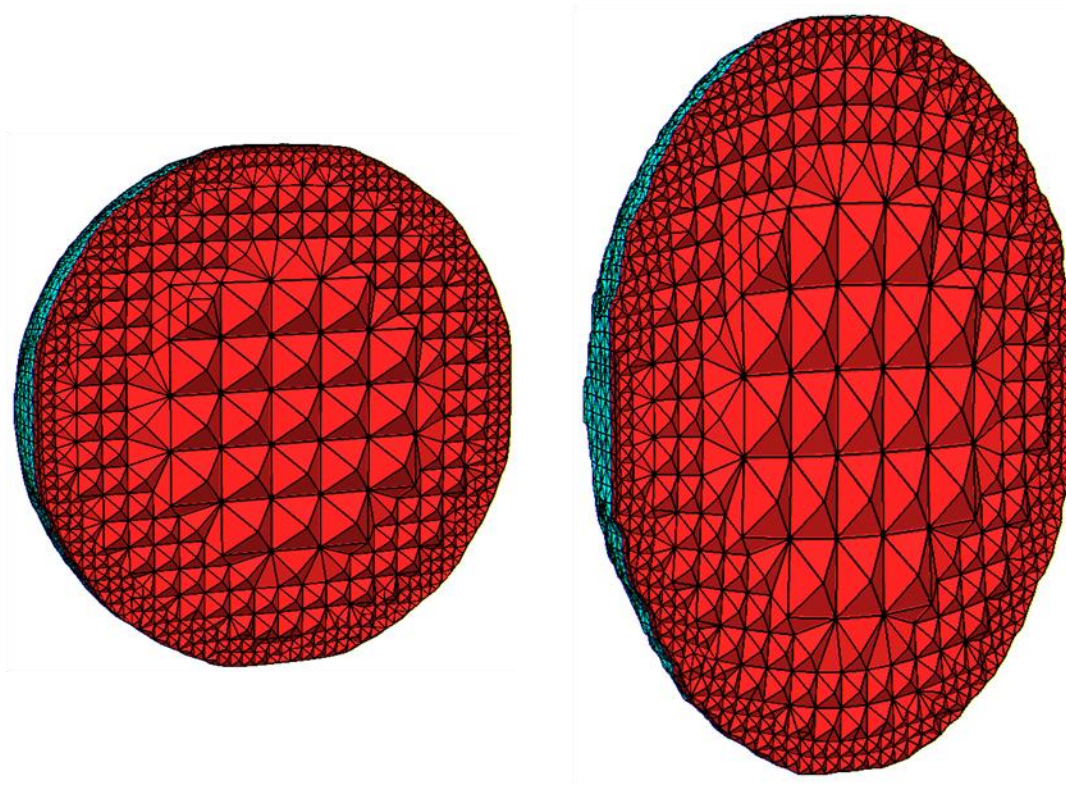


Figure 1. The mesh of a sphere is given on the left and morphed mesh into an ellipse is shown on the right. Both meshes are cut open to show the stretching that occurs to the tetrahedra within.

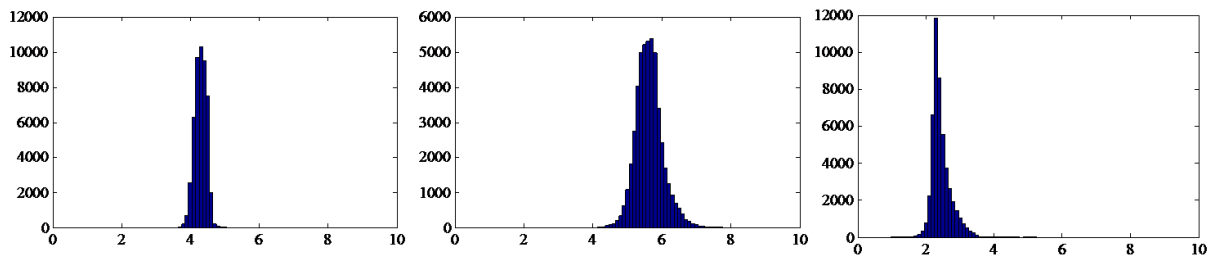


Figure 2. Histograms of the volume weighted deformation invariants that occur from morphing a sphere to an ellipse. J_1^c is left, J_2^c is center, and J_3^c is right. The values should be $J_1^c = 4.25, J_2^c = 5.5, J_3^c = 2.25$

Example 1

A sphere with equation:

$$(23) \quad x_1^2 + x_2^2 + x_3^2 < 20^2$$

is registered to an ellipsoid with equation:

$$(24) \quad \frac{x_1^2}{20^2} + \frac{x_2^2}{20^2} + \frac{x_3^2}{30^2} < 1$$

An example similar to this one is done in [33] and [7] where it is shown that the deformation is somewhat reasonable and/or better than another method. Here, we are able to achieve close to the exact minimum deformation. The difference between these two objects is unambiguous and should be used to understand what type of registration should occur, with one small caveat. The ellipse is stretched in the x_3 direction by 50%, which corresponds to two eigenvalues of the deformation gradient equal to 1.0 and one equal to 1.5. The caveat is that the sphere could rotate and then stretch and still produce a reasonable registration. However, here we analyze rotation invariant deformation measures which are unaffected by any rotation that may occur. An example of how this method rotates regions into the correct position in a case where the rotation is not ambiguous is given in example 2.

To draw a fair comparison to finite difference methods, the regions are voxelized with voxel size 1 by 1 by 1, which will introduce some error into the result. The registration is shown in figure 1. The invariants that are computed on each element cluster closely around the expected values, as shown in figure 2. We note that the invariants do not actually give the direction of the stretching as they are invariant to rotation.

Despite the apparent simplicity of this example, this is not a typical result for registration methods as explained in [33] and [34]. Methods such as [3] and [15] will produce large deformations that are not justified based on the images. In [33] and [34], these existing models are modified to produce a narrower range of volume change. The proposed method not only obtains similar results for volume change, but for measures of shear and stretch as well. This is important, as without these measurements it is unclear whether the registration method is causing unnecessary deformation. For example stretching might occur to keep the volume constant or as a side effect of forcing the images to match. A finite element based method [7] also does an example similar to this and does not obtain the correct result. A good deformation limiting regularization along with a matching term that does not distort volumes are not all that is required to obtain the correct deformation.

The superior result of the proposed registration method stems from how little the method does to match the images. No node is forced into any particular location (as is done in [7]), no fixed vector is involved ([33]), and no unnecessary volumetric movement is created ([15]). The mesh simply has to stay exactly on the corresponding target region and is free to achieve a deformation minimizing configuration while doing so.

This example is also suggestive of why statistically analyzing the deformation, rather than the shapes themselves, may be more informative. To figure out volume or stretch differences in the ellipsoids directly involves a global computation, such as an integral over the whole volume. In contrast, looking at the deformation gives you the stretch and volume difference by examining only a few elements, and theoretically only one. In this example, the image differences could be obtained either way. But for complicated registrations, like example 3 below, every element might have a different value relating in some way to the global differences between the initial and target image.

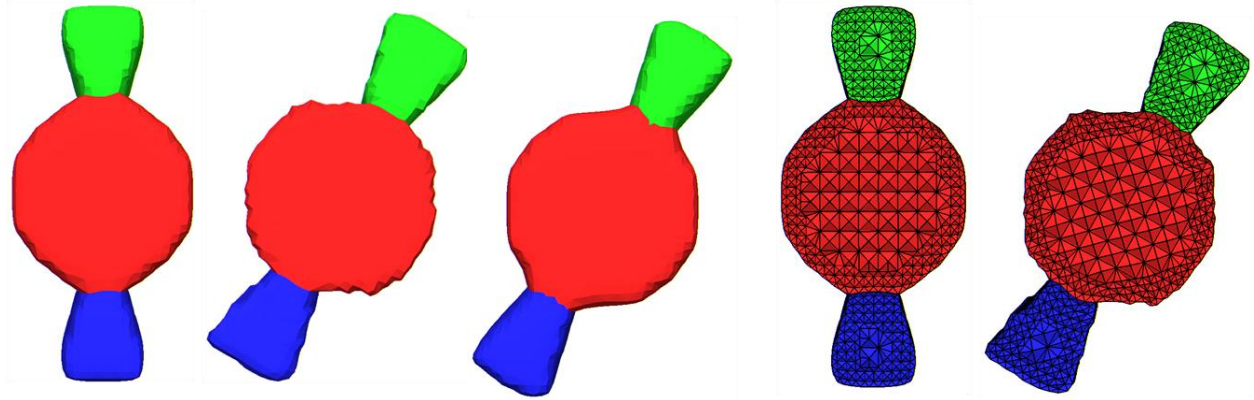


Figure 3. A mesh of the initial image is shown on the left, the morphed mesh on the center left, and a mesh of the target image is shown in the center. To show the rotation that occurs throughout the volume the initial mesh is cut open on the center right and the morphed mesh on the right. Region 1 is red, region 2 is green, and region 3 is blue.

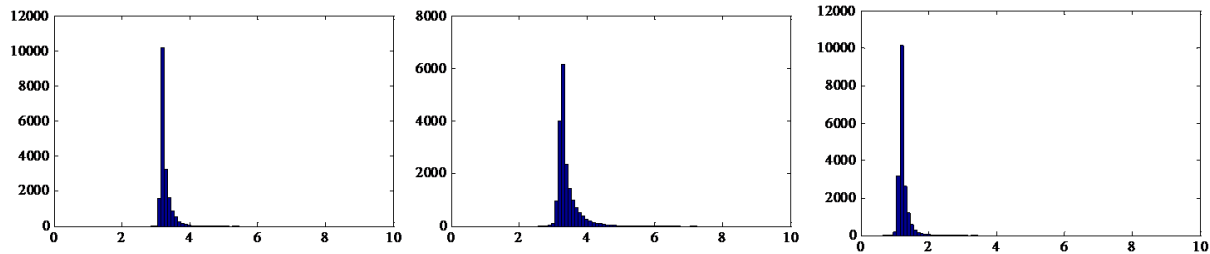


Figure 4. Histograms of the volume weighted deformation invariants that occur from the morphing in example 2. J_1^C is left, J_2^C is center, and J_3^C is right. The values should be $J_1^C = 3, J_2^C = 3, J_3^C = 1$

Example 2

Two images with three regions each that differ by a rotation are registered. Figure 3 shows two coordinates of the images and the image is constant in the third coordinate. While there are certainly easier methods for doing a rigid registration (that is, methods exist that characterize the rigid registration by 6 numbers instead of an arbitrary map), we chose this example because the resulting registration is completely unambiguous and can therefore be used to determine if the proposed registration method produces the correct result.

This type of behavior is important in real medical imaging examples, such as example 3 below, where only part of an object may differ by a rotation and a rigid alignment is consequently not possible as a first step before applying a non-rigid registration method. Considered as a non-rigid problem, matching the initial and target images correctly is quite difficult. Region 1, the tube, when considered on its own, already matches perfectly. For regions 2 and 3, there is no overlap between the initial and target images. The common practice of determining how all the boundary nodes of each region should move separately and in advance and then performing a volumetric registration as a second step will not work. Determining how the boundaries of regions 2 and 3 should be moved cannot be done by a simplistic procedure involves finding the nearest boundary in the target image but may be possible with a more sophisticated technique. But any reasonable boundary registration of region 1 will cause it to stick in place, as it already matches perfectly, and hence the correct volumetric registration of all three regions would be resisted.

The proposed method is capable of registrations of this type. Regions 2 and 3 in the mesh correctly find their corresponding regions in the target image and region 1 does not resist rotation caused by movement of regions 2 and 3. The mesh is cut open in figure 3 to show the large correctly rotated tetrahedra on the interior. The deformation near the boundary is slightly off because a voxelized version of a tube is being used. The deformation is given in figure 4 which roughly corresponds to no change in the rotationally invariant deformation measures.

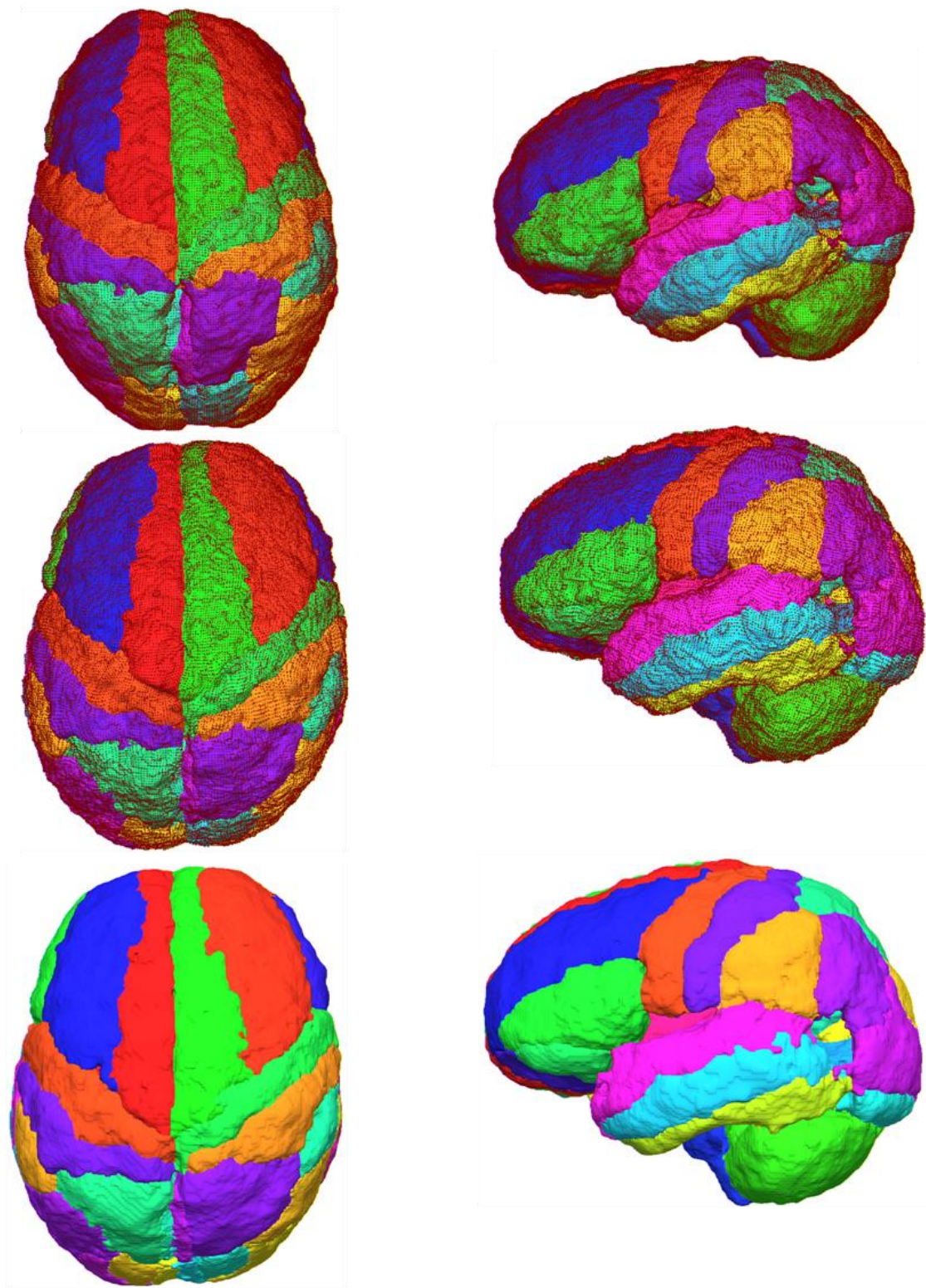


Figure 5A. Two views are shown from registration #1 in example 3. A mesh from the initial image is shown on the top, the morphed mesh is in the center, and a mesh of the target image is shown on the bottom. Boundary nodes are shown on the initial and morphed mesh to visualize the deformation that occurs on the surface.

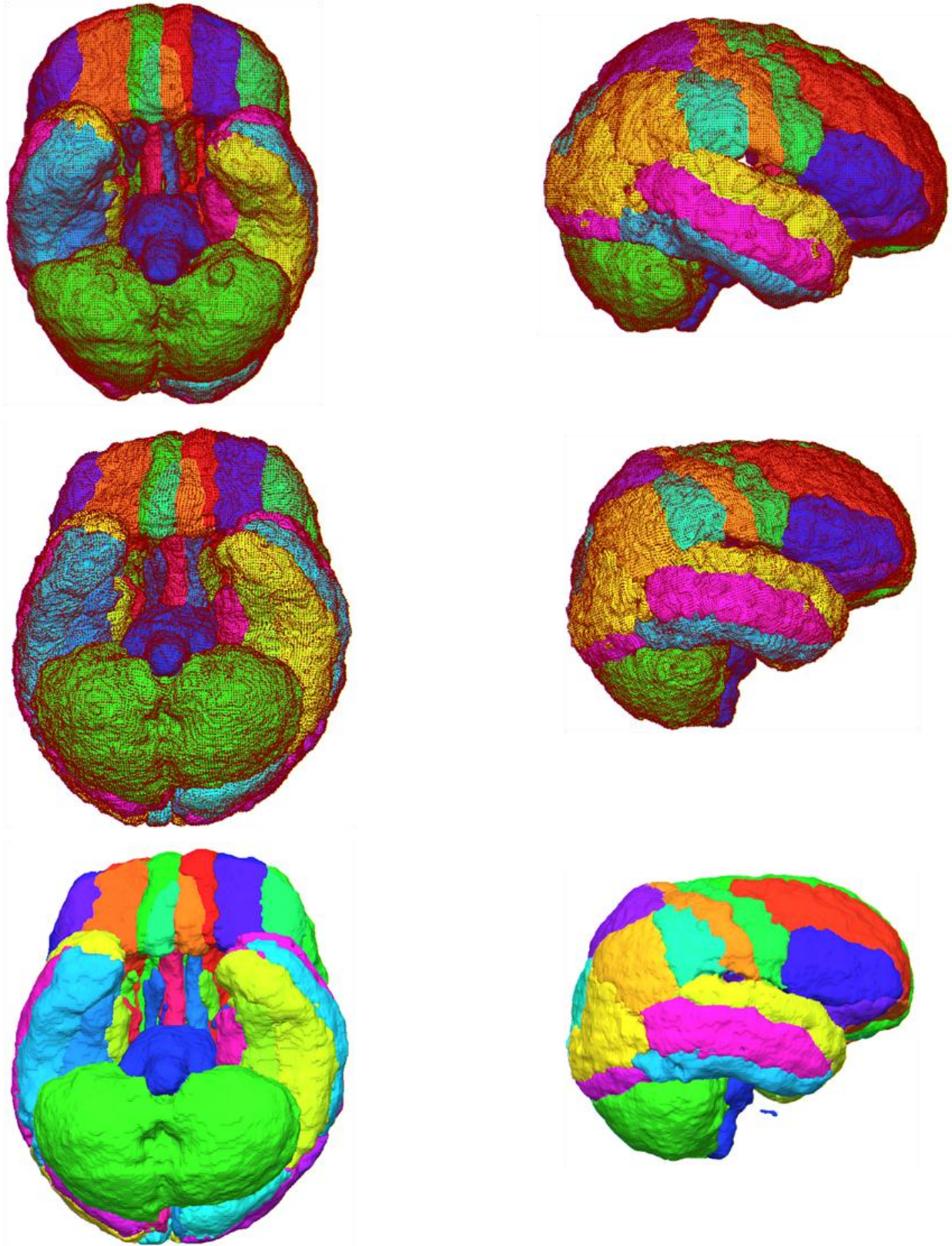


Figure 5B. Same as figure 5A but for registration #2 in example 3.

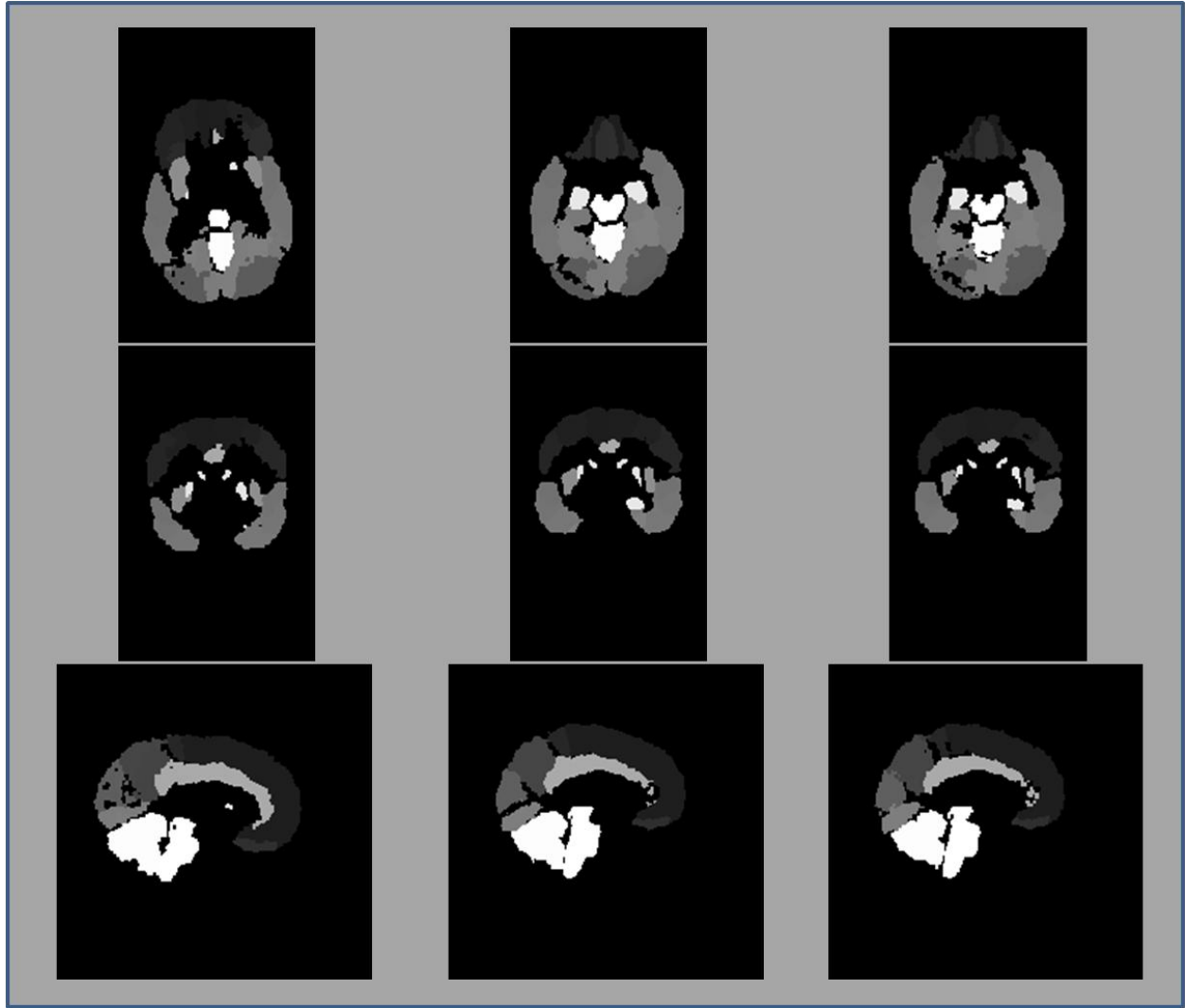


Figure 6A. Three cuts are made through the exact center of three 3D images relating to registration #1 in example 3. The left column shows three cuts of the initial image, the center column shows three cuts of the morphed image, and the right column shows 3 cuts of the target image.

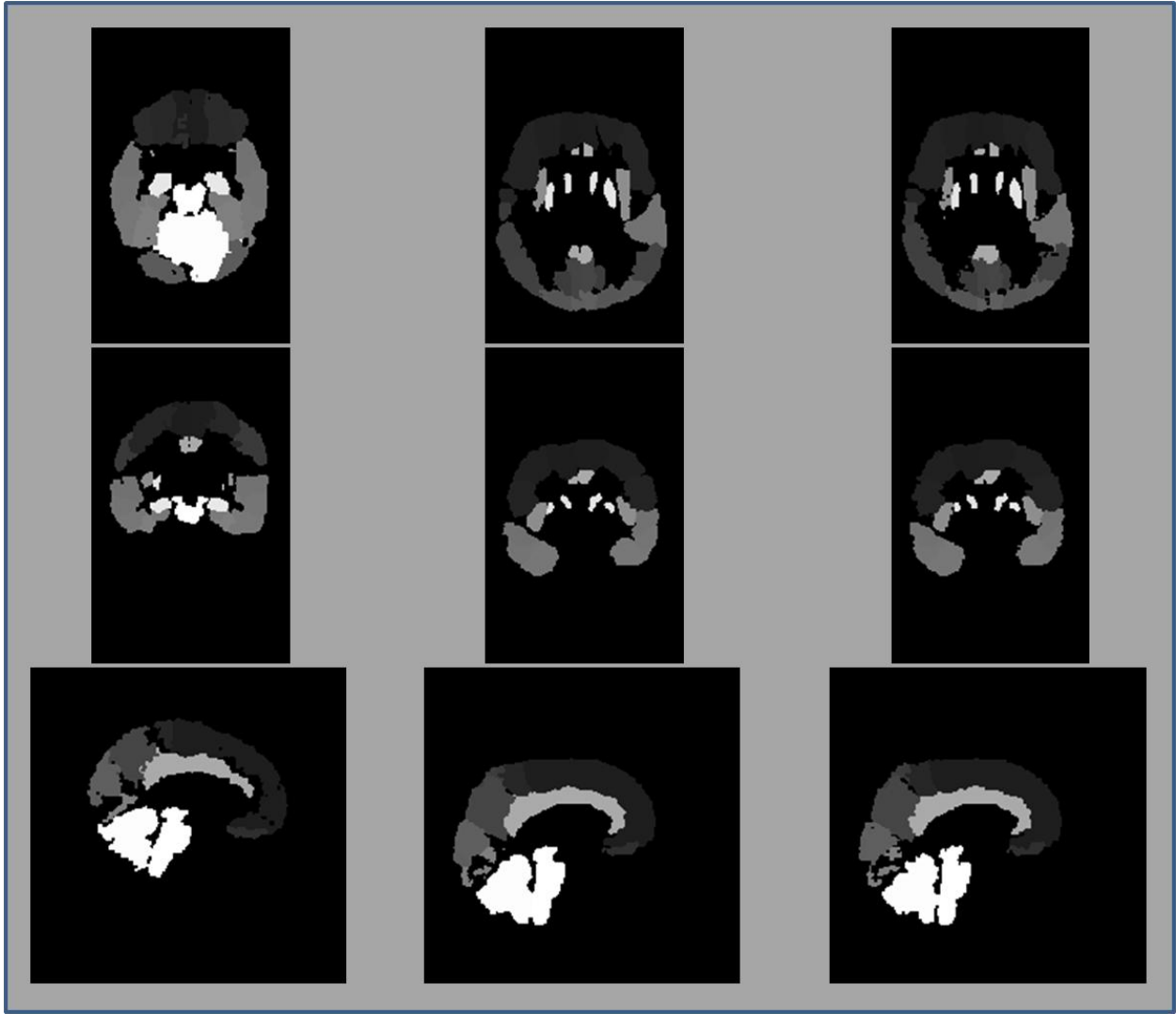


Figure 6B. The same as figure 6A but for registration #2 in example 3.

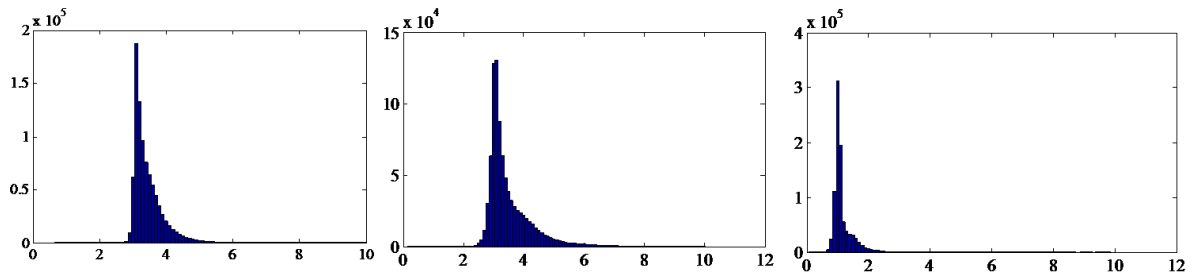


Figure 7A. Histograms of the volume weighted deformation invariants that occur from the morphing in registration #1 in example 3. J_1^C is left, J_2^C is center, and J_3^C is right.

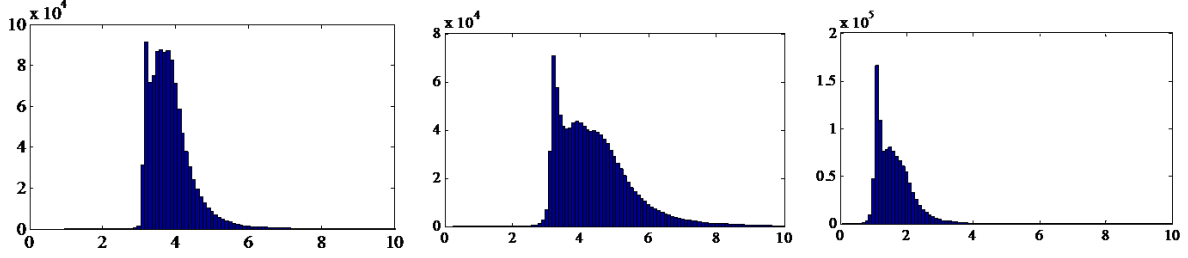


Figure 7B. Same as figure 7A but for registration #2 in example 3.

Example 3

Four automatically segmented brains were generated from the LONI pipeline ([5] and [30]) and used for two registration examples as shown in figures 5,6, and 7. For each of the 56 regions we computed the Dice coefficient of a target region, I_m , and a morphed region B_m .

$$(25) \quad D_m(I_m, B_m) = \frac{2|I_m \cap B_m|}{|I_m| + |B_m|} \in [0,1]$$

The computation involves both voxels, from the target region, and tetrahedra, from the morphed region. To convert the mesh to an image, we approximated the amount of mesh volume in each image voxel by assuming all the volume of each tetrahedron is located at tetrahedron's centroid. The voxel is assigned to the region with the most associated mesh volume. This voxelized image is then compared to the target image to obtain the dice coefficients. This process of transforming an image into a mesh and then back into an image does introduce some error in the dice coefficients. The Dice coefficients of every region before and after registration are given in table 1. Dice coefficients from before the registration were computing by simply using the images and no mesh. Figure 5 shows the initial and morphed meshes with the boundary nodes present to show the type of deformation that occurs. A separately generated mesh of the target image is shown for comparison. Figure 6 shows the initial image, the approximation to the morphed mesh and the target image. The invariants of the deformation are given in figure 7. Overall, we note that despite the significant differences between the initial and target images, the morphed and target images match very well. This is achieved using a very small amount of deformation as revealed in the histograms.

Registration methods that do not incorporate automatic anatomical segmentations into the method will sometime use manual segmentations afterward to evaluate the effectiveness of their methods ([20] and [26]). The overlap measures are not as good as those presented here. A critical comparison to these other methods which have a somewhat different validation technique would not be appropriate, but clearly, these results indicate that an effective means of incorporating the data in an accurate automatic structural segmentation has the potential to improve a brain registration.

Region Number	Before Registration #1	After Registration #1	Before Registration #2	After Registration #2
1	0.548771	0.963498	0.0509844	0.969764
2	0.580495	0.967291	0.0545999	0.970443
3	0.54279	0.968299	0.0266322	0.973716
4	0.577491	0.962209	0.000561246	0.962836
5	0.288413	0.972855	0.00537836	0.962104
6	0.407447	0.953972	0.0614528	0.956338
7	0.534865	0.954091	0	0.961055
8	0.539107	0.940693	0	0.949021
9	0.00016919	0.952389	0	0.957158
10	0	0.940602	0.0691253	0.956071
11	0.0521301	0.960743	0	0.956508
12	0.0365042	0.90987	0.00044238	0.928571
13	0	0.935214	0.000672947	0.937462
14	0	0.912787	0	0.933204
15	0.454753	0.945737	0	0.946345

16	0.565737	0.953927	0	0.953807
17	0.663397	0.948637	0	0.962624
18	0.714081	0.959789	0	0.963628
19	0.538618	0.938267	0	0.942461
20	0.749147	0.945187	0	0.936019
21	0.644427	0.937124	0	0.93813
22	0.715833	0.950787	0	0.945322
23	0.668487	0.953278	0	0.951349
24	0.707502	0.93896	0	0.952415
25	0.517688	0.923077	0	0.914426
26	0.481457	0.907959	0	0.915846
27	0.643303	0.934466	0	0.928032
28	0.423287	0.926505	0	0.92989
29	0.460316	0.928223	0	0.937523
30	0.39356	0.953376	0	0.937192
31	0.440258	0.882726	0	0.923407
32	0.557796	0.911304	0	0.919326
33	0.209502	0.943338	0	0.950533
34	0.452653	0.948294	0	0.959092
35	0.140926	0.956573	0	0.9596
36	0.416593	0.948222	0	0.953611
37	0.124486	0.946887	0	0.955689
38	0.258558	0.953847	0.000224936	0.950499
39	0	0.929159	0	0.941058
40	0.0127772	0.945515	0	0.947778
41	0.56823	0.910139	0	0.922782
42	0.570833	0.938658	0	0.930282
43	0.149778	0.921458	0	0.94171
44	0.263297	0.951295	0	0.941581
45	0.155711	0.953333	0	0.953378
46	0.148088	0.942894	0	0.935013
47	0.317376	0.915761	0	0.916346
48	0.419122	0.941777	0	0.943609
49	0.00624721	0.941071	0	0.944007
50	0.0232981	0.926679	0	0.92291
51	0	0.931634	0	0.910251
52	0	0.942614	0	0.930206
53	0	0.911073	0	0.946697
54	0	0.945243	0	0.944696
55	0.647841	0.981408	0.0309923	0.982277
56	0.49395	0.970592	0.162201	0.967213

Table 1. The dice coefficients before and after registration are shown for each region and for two registrations in example 3.

Conclusion:

We presented here a means to effectively incorporate an automatic segmentation into a registration method. The finite element implementation, with region matching and regularization terms in a single energy, produces excellent deformation minimizing and region matching results. Two academic examples produced the correct registration and examples with real brain data produced the expected results of the method.

The brain registration example given utilizes only one particular anatomical brain segmentation. We believe other brain, and non-brain, anatomical segmentations could be used. While these methods are not easy to develop and any error in the segmentation will also end up in the registration, some means of incorporating anatomical data is essential for an anatomical registration.

In a future work, we plan to further validate the method by considering how well hidden manual information is matched. We will then apply this registration method to the study of neurological disease.

Acknowledgements:

This work is funded by the National Institutes of Health through P41 RR013642 and the NIH Roadmap for Medical Research, Grant U54 RR021813. Information on the National Centers for Biomedical Computing can be obtained from <http://www.NCBCs.org>.

References:

- [1] Brock, K., Sharpe, M., Dawson, L., Kim, S. and Jaffray D "Accuracy of finite element model-based multi-organ deformable image registration" *Med. Phys.* 32, 1647 (2005); doi:10.1118/1.1915012
- [2] Chan, T., Vese, L.: Active Contours Without Edges. *IEEE Trans. Image Process.* 10(2), 266-277 (2001).
- [3] Christensen, G., Rabbitt, R., and Miller, M. (1996). Deformable templates using large deformation kinematics. *IEEE Transactions on Image Processing*, 5(10):1435–1447.
- [4] Cohen-Or, D. et al., "Three Dimensional Distance Field Metamorphosis" *ACM Transactions on Graphics*, Vol. 17, No. 2 116-141 (1998)
- [5] Dinov, I. et al. "Efficient, Distributed and Interactive Neuroimaging Data Analysis Using the LONI Pipeline" *Neuroinformatics* 3, 22 (2009).
- [6] Ferrant, M. et al. 3D Image Matching Using a Finite Element Based Elastic Deformation Model. *Lecture Notes in Computer Science* Vol 1679, 202-209 (1999).
- [7] Ferrant M., Warfield S.K., Nabavi A., Jolesz F.A., Kikinis R. Registration of 3D Intraoperative MR Images of the Brain Using a Finite Element Biomechanical Model. *Int Conf Med Image Comput Assist Interv.* 2000;3:19-28.
- [8] Gosz, Michael, *The Finite Element Method: Applications in Solids, Structures, and Heat Transfer*, Taylor & Francis, 2006.
- [9] Hughes, T., *The Finite Element Method: Linear Static and Dynamic Finite Element Analysis*, Prentice Hall, 1987.
- [10] Irving G., et al., "Invertible Finite Elements for Robust Simulation of Large Deformations" *Proceedings of the 2004 ACM SIGGRAPH/Eurographics symposium on Computer animation*, 131-140 (2004).
- [11] Jifeng, N. et al. "NGVF: An improved external force field for active contour model". *Pattern Recognition Letters* 28, 58-63 (2007)
- [12] Joshi, A. A. et al., "Surface-constrained Volumetric Brain Registration Using Harmonic Mappings", *IEEE Trans. Med. Imag.*, Vol 26, no 12 pp 1657-1669, 2007
- [13] Joshi, A., Lederman, C., Dinov, I., Van Horn, J., Toga A., "A Combined Approach for Surface and Volume based Registration and Morphometry using Tetrahedral Meshes " (submitted).
- [14] Jung M., Chung G., Sundaramoorthi G., Vese L., and Yuille A.L., Sobolev gradients and joint variational image segmentation, denoising and deblurring, *SPIE Electronic Imaging Conference Proceedings, Computational Imaging VII, SPIE Vol. 7246*, 2009
- [15] Le Guyader, C., Vese, L.: A Combined Segmentation and Registration Framework with a nonlinear Elasticity Smoother. *UCLA C.A.M. Report 08-16* (2008).
- [16] Lederman, C., Joshi A., Dinov I., Vese, L., Toga, A., Van Horn, J.D., The generation of tetrahedral mesh models for neuroanatomical MRI, *NeuroImage*, In Press, Uncorrected Proof, Available online 10 November 2010, ISSN 1053-8119, DOI: 10.1016/j.neuroimage.2010.11.013

- [17] Lie, J., et al. "A piecewise constant level set framework" *International Journal of Numerical Analysis and Modeling*. Volume 2, Number 4, pages 422-438 (2005)
- [18] Moeller, M. Wittman, T., and Bertozzi, A.L., "A variational approach to hyperspectral image fusion," *SPIE Conference on Defense, Security, and Sensing 2009*, April 2009
- [19] Neuberger, J.: *Sobolev Gradients and Differential Equations*. Springer (1997)
- [20] Postelnicu et al., "Combined Volumetric and Surface Registration." *IEEE Trans. On Medical Imaging*. Vol 28, pp 508-522 (2009)
- [21] Pedregal, P. "Variational Methods in Nonlinear Elasticity" *Society for Industrial and Applied Mathematics* (2000).
- [22] Pohl K. M, Fisher, J. Grimson, W.E.L., Kikinis, R., and Wells, W.M.. "A bayesian model for joint segmentation and registration." *NeuroImage*, 31(1), pp. 228-239, 2006
- [23] Renka, R.: "Constructing Fair Curves and Surfaces with a Sobolev Gradient Method." *Computer Aided Geometric Design* 21, 137-149 (2004)
- [24] Schnabel, J., Tanner, C., Castellano-Smith A., Degenhard, A., Leach M., Hose R., Hill, D., Hawkes, J. "Validation of Nonrigid Image Registration Using Finite-Element Methods: Application to Breast MR Images" *IEEE Transactions on Medical Imaging*, Vol. 22, No. 2, February 2003
- [25] Sethian J. "A Fast Marching Level Set Method for Monotonically Advancing Fronts." *Proc. Natl. Acad. Sci.*, vol. 93, 1591–1595, 1996
- [26] Shen, D. and Davatzikos, C., "Hammer: Hierarchical attribute matching mechanism for elastic registration," *IEEE Trans. Med. Imag.*, vol. 21 no. 11 pp. 1421-1439 Nov. 2002.
- [27] Tarantola A, "Inverse Problem Theory" *Society for Industrial and Applied Mathematics* (2004)
- [28] Teran, J. et al.: "Robust Quasistatic Finite Elements and Flesh Simulation." *Symposium on Computer Animation*. 181-190 (2005).
- [29] Thompson, P. M., Giedd, J. N., Woods, R. P., MacDonald, D., Evans, A. C., and Toga, A. W. (2000). "Growth patterns in the developing brain detected by using continuum mechanical tensor maps." *Nature*, 404(6774):190–3.
- [30] Tu, Z. et al. "Brain Anatomical Structure Segmentation by Hybrid Discriminative/Generative Models" *IEEE Transactions on Medical Imaging* Vol 10 (2005)
- [31] Unal, G. et al., "Coupled PDEs for Non-Rigid Registration and Segmentation" *IEEE Computer Society Conference on Computer Vision and Pattern Recognition* (2005)
- [32] Weatherill N.P., Hassan O. "Efficient Three-Dimensional Delaunay Triangulation with Automatic Point Creation and Imposed Boundary Constraints." *Int. J. for Num. Meth. in Eng.*, vol. 37, 2005–2039, 1994
- [33] Yanovsky, I. et al. "Log-unbiased Large Deformation Image Registration." *VISAPP 1*, 272-279, 2007
- [34] Yanovsky, I. et al. "Nonlinear Elastic Registration with Unbiased Regularization in Three Dimensions" *MICCAI 2008*.
- [35] Yezzi, A., Zöllei, L., Kapur, T. "A variational framework for integrating segmentation and registration through active contours", *Medical Image Analysis*; Volume 7, Issue 2, June 2003, Pages 171-185.